Physicochem. Probl. Miner. Process., 62(6), 2026, 242327

http://www.journalssystem.com/ppmp

Physicochemical Problems of Mineral Processing

ISSN 1643-1049
© Wroclaw University of Science and Technology

Control of slag composition in matte smelting process of high-magnesium nickel sulfide concentrate

Youhao Zeng [1,2], Xubin Wang [3], Haipei Zhang [1,2], Bo Li [1,2], Yonggang Wei [1,2], Shichao Wu [1,2], Hairong Zhou [3], Zelei Gao [3]

[1] Faculty of Metallurgical and Energy Engineering, Kunming University of Science and Technology, Kunming 650093, China

[2] State Key Laboratory of Complex Nonferrous Metal Resources Clean Utilization, Kunming University of Science and Technology, Kunming 650093, China

[3] Jinchuan Group Nickel and Cobalt Co., LTD, Jinchang 737100, China

Corresponding author: 510268053@qq.com (Haipei Zhang), libokmust@163.com (Bo Li)

Abstract: As high-grade nickel sulfide concentrates become increasingly scarce, high-magnesium nickel sulfide concentrates will become the primary feedstock for pyrometallurgical nickel production. High magnesium content can lead to issues such as unreasonable slag composition, high slag viscosity, and high nickel losses during the smelting process; existing processes struggle to meet the smelting requirements of high-magnesium nickel sulfide concentrates. To address these issues, this study investigated the reaction mechanisms during the matte smelting of high-magnesium nickel sulfide concentrates. It examined the effects of key parameters – including nickel-matte grade, temperature, Fe/SiO_2, and CaO/SiO_2 ratios – on slag phase composition, physical properties, and nickel loss, thereby identifying optimal slag compositions and process parameters. The results indicate that under optimal process conditions (nickel matte grade of 35%, temperature of 1425°C, Fe/SiO_2 ratio of 0.8, and CaO/SiO_2 ratio of 0.15), the nickel content in the slag can be reduced to 0.27 wt.%. These results meet industrial production standards, achieve efficient nickel enrichment and provide a theoretical basis and practical guidance for ensuring the smooth operation of the smelting process for high-magnesium nickel concentrates.

Keywords: high-magnesium nickel sulfide concentrate, Matte smelting, slag composition control, nickel loss

1. Introduction

Nickel is a vital industrial metal and a fundamental raw material for military manufacturing, including the production of aircraft and radar. It is also an indispensable strategic resource for developing emerging industries (Zhao et al., 2022; Elshkaki et al., 2017). Nearly 40% of the world's nickel resources occur in the form of sulfide ores, and pyrometallurgical extraction from sulfide concentrates is the primary method of nickel production (Wang et al., 2020; Faris et al., 2022; Mudd, 2010). As reserves of high-grade nickel sulfide concentrates continue to be depleted, the concentrates is increasingly characterized by high magnesium content and low nickel content (Mu et al., 2019; Lin et al., 2025; Qin et al., 2009; Zhen et al., 2009). During the smelting of high-magnesium nickel sulfide concentrate to produce matte, problems such as high slag viscosity and poor slag fluidity arise. These problems hinder the smelting process and lead to difficulty in slag-matte separation, resulting in increased nickel loss in the slag (Piskunen et al., 2017; Sukhomlinov et al., 2019; Zhang et al., 2023). The nickel loss in the smelting slag can reach as high as 1%. Therefore, reducing nickel loss during the matte smelting process of high-magnesium nickel sulfide concentrate, while ensuring that the smelting process proceeds smoothly, has become a critical issue that must be addressed.

During nickel smelting, nickel losses associated with the slag phase generally occur through two mechanisms: chemical dissolution and physical entrainment. Chemically dissolved nickel is mainly

DOI: 10.37190/ppmp/242327

present in the slag in the form of nickel oxide, whereas mechanically entrained nickel is primarily associated with matte droplets that fail to settle completely and remain trapped within the slag layer (Henao et al., 2022; Sun et al., 2021). Increasing the smelting temperature is an effective way to reduce nickel loss. The composition of nickel slag is also a major factor affecting its physicochemical properties and nickel loss. Controlling the Fe/SiO_2 ratio within the slag provides an effective strategy for adjusting slag composition, reducing slag viscosity, and decreasing mechanical entrainment loss of nickel in the slag. SiO_2 generally serves as a slag-forming oxide and forms low-melting silicates with basic oxides such as FeO and MgO, thereby facilitating slag melting. Meanwhile, SiO_2 features a low density of 2.5 g/cm^3. Reducing the Fe/SiO_2 ratio can decrease the density of slag and facilitate the separation between slag and nickel matte (Wang etal., 2023; Zhang et al., 2022; Wang et al., 2021; Wang et al., 2022). CaO is a crucial component in the slag formation process (Wang et al., 2020; Shen et al., 2019). Appropriate addition of CaO can improve the physicochemical properties of the slag, reduce slag viscosity, and decrease nickel loss in the slag.

Various approaches have been investigated to address the challenges associated with low-grade, high-magnesium nickel sulfide resources. One strategy involves the removal of Mg-bearing silicate gangue minerals prior to smelting. However, serpentine and other Mg-bearing minerals tend to interact with pentlandite during flotation, making their efficient separation difficult (Feng et al., 2016; Lu et al., 2017; Lu et al., 2017). Alternative thermal treatment methods have also been explored. For example, Wang et al. (2024) proposed a thermal upgrading process involving metallic iron addition, in which Ni was preferentially transferred into a Ni–Fe alloy and subsequently recovered by magnetic separation. Other approaches, such as low-temperature roasting followed by selective decomposition and water leaching, have also been investigated for nickel recovery from sulfide resources (Mu et al., 2019). Nevertheless, these processes generally require additional pretreatment, reductant addition, or separation steps. Matte smelting remains a reliable processing route due to its high throughput, relatively short processing time, and ability to simultaneously recover valuable metals such as Cu and Co. However, relatively few studies have systematically investigated the phase transformations, slag structural evolution, and changes in slag physicochemical properties during the matte smelting of high-magnesium nickel sulfide concentrates.

In summary, this study investigates the reaction behavior, phase evolution, and changes in physicochemical properties during the matte smelting process of high- magnesium nickel sulfide concentrates. The effects of key parameters including nickel matte grade, temperature, Fe/SiO_2 ratio, and CaO/SiO_2 ratio on nickel content in slag are clarified. The slag composition is optimized to achieve low viscosity and low nickel loss in the slag. This work addresses the problem of excessive nickel loss in slag during the matte smelting of high-magnesium nickel sulfide concentrate and provides a reliable theoretical basis for the subsequent pyrometallurgical treatment of such concentrates.

2. Materials and characterization

2.1. Materials

The raw material adopted in this study is a nickel sulfide concentrate sourced from a nickel-cobalt enterprise in China. The elemental analysis results of this nickel sulfide concentrate are presented in Table 1. It contains 13.66 wt.% magnesium oxide, 3.99 wt.% nickel, and 2.52 wt.% copper. The Fe(Total) content of the concentrate was 27.08 wt.%, including the Fe present in Fe_3O_4, while the Fe_3O_4 content was independently measured to be 8.20 wt.%. Therefore, this concentrate is categorized as a nickel sulfide concentrate with a high magnesium content. The phase composition and surface morphology of the nickel sulfide concentrate were characterized by XRD and SEM, with the corresponding results presented in Fig. 1(a) and Fig. 1(b), respectively. The SEM images reveal that the distribution of nickel, copper, and iron in the nickel sulfide concentrate is highly overlapped with that of sulfur, while the distribution of magnesium is highly consistent with oxygen and silicon. Accordingly, nickel, copper, and iron mainly exist in the form of sulfides in the nickel sulfide concentrate, and magnesium oxide predominantly occurs as silicate minerals. Combined with the XRD analysis and SEM microstructure results, the main mineral phases of the nickel sulfide concentrate are identified as pentlandite ($Fe_9Ni_9S_{16}$), chalcopyrite ($CuFeS_2$), pyrite ($FeS_{2)}$, and pyrrhotite (Fe_7S_8). Magnesium oxide is mainly

present in the concentrate in the form of silicate minerals such as serpentine ($Mg_3Si_2O_5(OH)_4$) and talc ($Mg_3Si_4O_{10}(OH)_2$).

Table 1. Chemical composition analysis of nickel sulfide concentrate

Component	Ni	Co	Cu	Fe (total)	S
Mass percent	3.99	0.11	2.52	27.08	17.24
Component	CaO	MgO	SiO_2	Al_2O_3	Other
Mass percent	1.16	13.66	19.15	1.87	13.22

** The Fe_3O_4 content in high-magnesium nickel sulfide ore is 8.20 wt.%.*

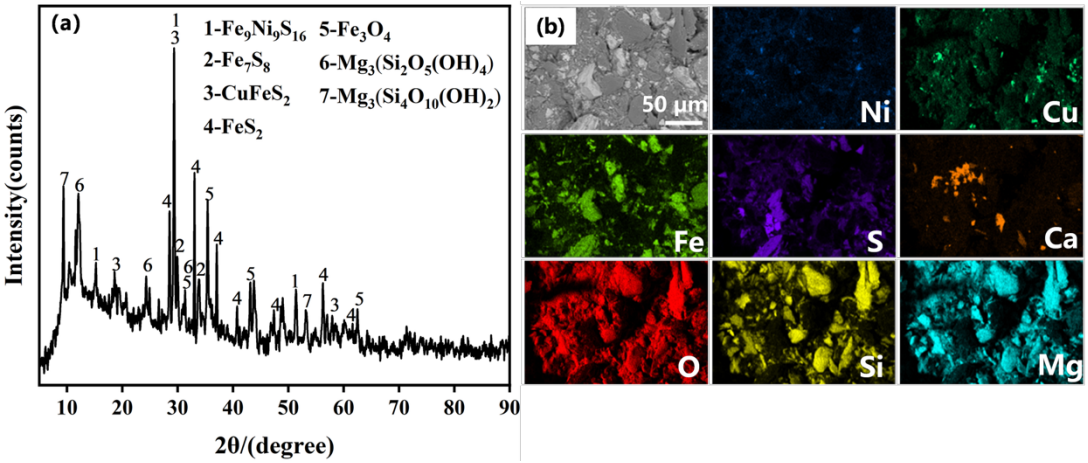


Fig. 1. Characterization of high-magnesium nickel sulfide concentrate: (a) XRD pattern; (b) SEM micrograph

2.2. Experimental methods

The experimental equipment and analytical methods are shown on Fig. 2. To investigate the effects of key parameters, including nickel matte grade, temperature, Fe/SiO_2 ratio, and CaO/SiO_2 ratio, on the smelting behavior of high-magnesium nickel sulfide concentrate, 100 g of nickel sulfide concentrate was thoroughly mixed with additives at predetermined ratios and subsequently transferred to a crucible for smelting experiments. The crucible was introduced into a high-temperature furnace, and the sample temperature was increased to 1400–1500 °C following a heating ramp of 6 °C/min. To ensure complete melting of the charge, the mixture was maintained under constant-temperature conditions for a duration of 30 min. Subsequently, an O_2–N_2 gas mixture with an oxygen enrichment of 70 vol.% was injected into the melt through a top-blowing lance. The relatively high oxygen enrichment was selected to intensify sulfide oxidation while reducing the introduction of inert N_2, thereby improving heat utilization and smelting intensity. During blowing, O_2 and N_2 were continuously supplied at flow rates of 280 and 120 mL/min, respectively, using flow meters, and the gas flow rates were maintained constant throughout the blowing stage. The theoretical oxygen requirement was determined according to the intended matte grade, and the corresponding theoretical blowing time was calculated from the O_2 flow rate. Because the oxygen requirement varies with the intended matte grade, the theoretical blowing time was not identical for all experiments. Under the condition corresponding to a matte grade of 35%, the calculated theoretical blowing time was approximately 18 min. This theoretical value was used as a reference for controlling the blowing operation rather than as a fixed blowing duration for all experiments. The actual blowing duration was adjusted according to the oxygen requirement corresponding to the intended matte grade. Importantly, the matte grades reported in this study were experimentally determined rather than calculated from the theoretical blowing time or the supplied O_2 volume. After smelting, the Ni and Cu contents of the produced matte were determined by chemical analysis, and the sum of the measured Ni and Cu contents was taken as the experimental matte grade. The experimentally obtained nickel matte grade was controlled to within

approximately ±1% of the target grade (At a targeted nickel matte grade of 35%, the matte grade obtained in the experiments was maintained within the range of 34–36%). Considering practical industrial operating conditions, after completion of oxygen blowing, the melt was held at the smelting temperature for an additional 30 min to promote slag–matte separation. The furnace was subsequently cooled to 700 °C at a controlled cooling rate of 5 °C/min, followed by natural cooling in the furnace to room temperature. The corresponding experimental parameters are listed in Table 2.

In this study, Fe/SiO_2 is defined as the mass ratio of elemental iron in the slag to the mass of SiO_2, and CaO/SiO_2 is defined as the mass ratio of CaO in the slag to the mass of SiO_2. Fe represents the total amount of iron entering the slag (not FeO, Fe_2O_3, Fe^{2+}, or Fe_3O_4). The amount of Fe entering the slag is calculated by the iron mass balance between the slag and the nickel matte, as shown in Eq. (A):

$$m_{Fe,Slag} = m_{TFe,feed} - m_{Fe,matte} \quad (A)$$

The Fe/SiO_2 ratio is calculated as shown in Eq. (B):

$$m_{Fe,slag}=m_{TFe,feed}-m_{Fe,matte} \quad (B)$$

The Fe/SiO_2 ratio is calculated as shown in Eq. (C):

$$R_{Fe/SiO_2} = m_{Fe,slag}/m_{SiO_2,total} \quad (C)$$

The CaO/SiO_2 ratio is calculated as shown in Eq. (D):

$$R_{CaO/SiO_2} = m_{CaO,total}/m_{SiO_2,total} \quad (D)$$

where, $m_{TFe,feed}$ denotes the total mass of Fe in the concentrate, $m_{Fe,matte}$ is the mass of Fe retained in the matte, predominantly in the form of FeS, $m_{SiO_2,total}$ is the total mass of SiO_2 contributed by both the concentrate and the added quartz, and $m_{CaO,total}$ is the total mass of CaO contributed by both the concentrate and the CaO addition.

Table 2. Experimental parameters for smelting of high-magnesium nickel sulfide concentrate

Experimental parameters	Parameter Range	Fixed Parameters			
		Grade	Temperature	Fe/SiO_2	CaO/SiO_2
Grade (%)	35, 37, 42, 45	-	1450 ℃	1.0	0.1
Temperature (℃)	1400, 142, 1450, 1475, 1500	35%	-	1.0	0.1
Fe/SiO_2	1.0, 0.9, 0.8, 0.75, 0.7	35%	1425 ℃	-	0.1
CaO/SiO_2	0.1, 0.15, 0.2, 0.25, 0.3	35%	1425 ℃	0.8	-

2.3. Characterization

Theoretical analyses were conducted using the thermodynamic simulation platform FactSage 8.1 and its integrated phase equilibrium, phase diagram, and viscosity calculation functions to investigate phase transformation behavior, physicochemical characteristics, and chemically dissolved nickel in nickel slag. For the FactSage equilibrium calculations, the Fe-bearing phases were reconstructed based on the elemental composition of the concentrate in combination with XRD and SEM characterization of the mineral phases. Iron sulfides were introduced into the calculation as $Fe_9Ni_9S_{16}$, $CuFeS_2$, FeS_2, and Fe_7S_8, whereas independently determined Fe_3O_4 was introduced separately as an oxide phase. MgO, SiO_2, CaO, and Al_2O_3 were also included according to the feed composition, together with O_2 and N_2 in amounts corresponding to the smelting conditions. For each calculation, the amounts of SiO_2 and CaO were adjusted according to the target experimental Fe/SiO_2 and CaO/SiO_2 ratios. FeO was not specified as an initial Fe-bearing phase in the input. Instead, it was generated during the thermodynamic equilibrium calculation as an oxide product resulting from the oxidation and equilibration of the Fe-bearing sulfide phases. X-ray diffractometer (RIGAKU TTR II-18KW) was adopted to conduct phase analysis on raw materials and slag samples. X-ray diffraction data were acquired in the 2θ region from 5° to 90° at a programmed scanning speed of 5°/min. The contents of

Ni, Cu, Co, TFe, S, MgO, SiO_2, CaO, and Al_2O_3 in the concentrate and slag were directly determined by chemical composition analysis. The Fe_3O_4 content in the raw materials and slag samples was measured using a SATMAGAN-135 magnetic analyzer (Rapiscan Systems, Finland), Other magnetic substances are present only in small amounts, so the measured value mainly reflects the Fe_3O_4 content. The measured total Ni content in slag includes both chemically dissolved Ni in the oxide/silicate slag matrix and Ni associated with mechanically entrained matte droplets. In this work, mechanically entrained Ni and chemically dissolved Ni were not separately quantified by chemical analysis. Instead, the content of chemically dissolved Ni was predicted using FactSage equilibrium calculations. Accordingly, the content of mechanically entrained Ni in the slag can be estimated using the following equation, as shown in Eq. (5):

$$w_{Ni,mech} = w_{Ni,total} - w_{Ni,diss,FactSage} \quad (5)$$

where $w_{Ni,total}$ represents the total Ni content in the experimentally obtained slag as determined by chemical analysis, $w_{Ni,diss,FactSage}$ represents the content of chemically dissolved Ni predicted by FactSage equilibrium calculations, and $w_{Ni,mech}$ represents the predicted content of mechanically entrained Ni in the slag.

SEM-EDS (SEM5000-xplore30) was used to characterize the micromorphology and phase distribution characteristics of raw materials and nickel slag. X-ray photoelectron spectroscopy (XPS) was employed to characterize the chemical states of iron in the slag. The relative contents and variations of Fe^{2+} and Fe^{3+} were analyzed by peak deconvolution of the high-resolution Fe 2p spectra. Fourier transform infrared (FTIR) spectroscopy was performed to characterize the structural features of slags with different CaO contents. A RHEOTRONIC-Ⅱ high-temperature viscometer was used to explore the influences of Fe/SiO_2 and CaO/SiO_2 mass ratios on slag viscosity. The melting properties of slags with varying Fe/SiO_2 and CaO/SiO_2 ratios were examined using a microcomputer intelligent ash melting point apparatus (TJHR-6000).

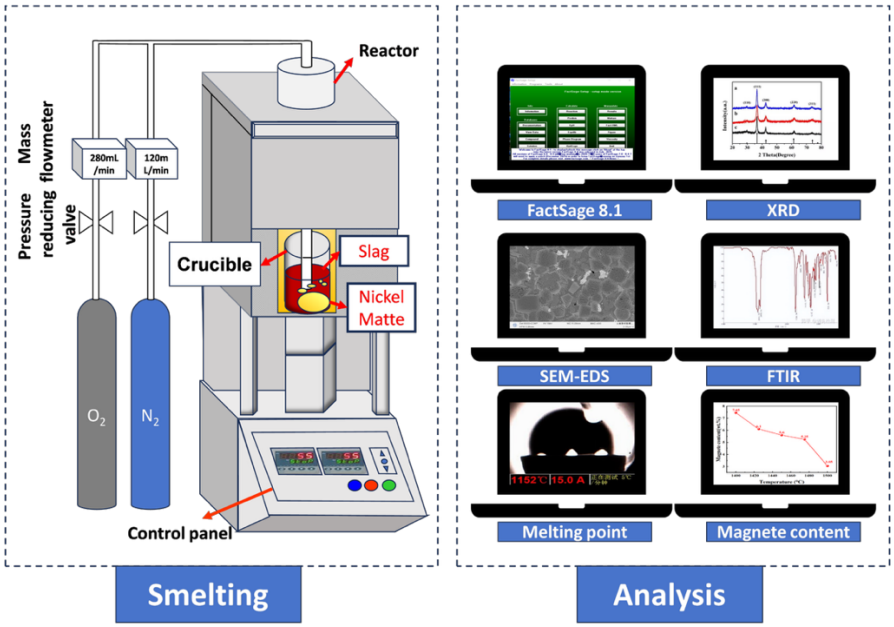


Fig. 2. Schematic diagram of the experimental apparatus and characterization techniques

3. Results and discussion

3.1. Reaction law of smelting process

The possible reactions involved in the matte smelting of high-magnesium nickel sulfide concentrate are listed as Eqs. (1) – (21) in Table 3. Thermodynamic calculations indicate that these reactions are thermodynamically feasible within the investigated temperature range, and the corresponding variations in Gibbs free energy with temperature are presented in Fig. 3. The matte-smelting process mainly involves the decomposition and oxidation of sulfides, followed by slag-forming reactions

between the resulting metal oxides and slag-forming components such as SiO_2 and CaO. Previous studies have shown that pentlandite, chalcopyrite, pyrite, and pyrrhotite can undergo decomposition and transformation during the heating of nickel sulfide concentrates (Yu et al., 2012; Božinović et al., 2011), and the possible reactions involved are represented by Eqs. (1) – (5). Under the investigated temperature conditions, the sulfides can be further oxidized by the injected O_2 to form metal oxides such as FeO, as represented by Eqs. (6) – (13). Meanwhile, FeO, MgO in the slag can further react with SiO_2 and CaO to form silicate phases such as Fe_2SiO_4, Mg_2SiO_4, $CaMgSi_2O_6$, and $CaFeSi_2O_6$, as represented by Eqs. (14) – (21). With the addition of SiO_2 and CaO, a greater proportion of Fe can be incorporated into silicate phases, thereby suppressing Fe_3O_4 formation to some extent. It should be emphasized that a negative ΔG value only indicates that a reaction is thermodynamically feasible under the specified conditions and does not necessarily imply that the reaction occurs to a significant extent during the actual smelting process. Therefore, the thermodynamic calculations in this study are primarily used to evaluate the feasibility of the proposed reaction pathways rather than determine the actual reaction extent or establish a strictly sequential reaction mechanism.

Table 3. Chemical reaction

Chemical Reaction	No.
$Fe_9Ni_9S_{16} = 1/2\ S_2 + 3\ Ni_3S_2 + 9\ FeS$	(1)
$2\ CuFeS_2 = Cu_2S + 2\ FeS + 0.5\ S_2$	(2)
$Fe_7S_8 = 7\ FeS + 0.5\ S_2$	(3)
$FeS_2 = FeS + 0.5\ S_2$	(4)
$3\ NiS = Ni_3S_2 + 1/2\ S_2$	(5)
$2\ CuFeS_2 + O_2 = Cu_2S + 2FeS + SO_2$	(6)
$2/7\ Ni_3S_2 + O_2 = 6/7\ NiO + 4/7\ SO_2$	(7)
$Fe_7S_8 + O_2 = 7\ FeS + SO_2$	(8)
$FeS_2 + O_2 = FeS + SO_2$	(9)
$2/3\ FeS + O_2 = 2/3\ FeO + 2/3\ SO_2$	(10)
$3/5\ FeS + O_2 = 1/5\ Fe_3O_4 + 3/5\ SO_2$	(11)
$2/7\ FeS + O_2 = 1/7\ Fe_2O_3 + 2/7\ SO_2$	(12)
$1/2\ S_2 + O_2 = SO_2$	(13)
$2\ FeO + SiO_2 = Fe_2SiO_4$	(14)
$2\ MgO + SiO_2 = Mg_2SiO_4$	(15)
$6\ FeO + O_2 = 2\ Fe_3O_4$	(16)
$CaO + MgO + 2\ SiO_2 = CaMgSi_2O_6$	(17)
$CaO + FeO + 2\ SiO_2 = CaFeSi_2O_6$	(18)
$3\ Fe_3O_4 + FeS + 5\ SiO_2 = 5\ Fe_2SiO_4 + SO_2$	(19)
$4\ Fe_3O_4 + 6\ CaO + O_2 = 6\ CaFe_2O_4$	(20)
$2\ Fe_2SiO_4 + CaO = CaFeSi_2O_6 + 3\ FeO$	(21)

3.2. Effect of nickel matte grade

The effect of nickel matte grade on nickel content in slag was investigated at 1450°C with $Fe/SiO_2 = 1.0$ and $CaO/SiO_2 = 0.10$. Fig. 4(a) and Fig. 4(b) present the cross-sectional morphologies of slag samples corresponding to different matte grades. As the nickel matte grade increases, the efficiency of nickel matte enrichment decreases. This is because higher grades require the injection of more oxygen, which raises the oxygen potential of the system. As a result, FeO is more easily oxidized into Fe_3O_4, which has a higher melting point, and the fluidity of the slag decreases, leading to reduced nickel-slag enrichment efficiency. The relationship between the nickel matte grade and both the Fe_3O_4 content in slag and the nickel content in slag is shown in Fig. 4(c). As the nickel matte grade increases, the Fe_3O_4 content in the

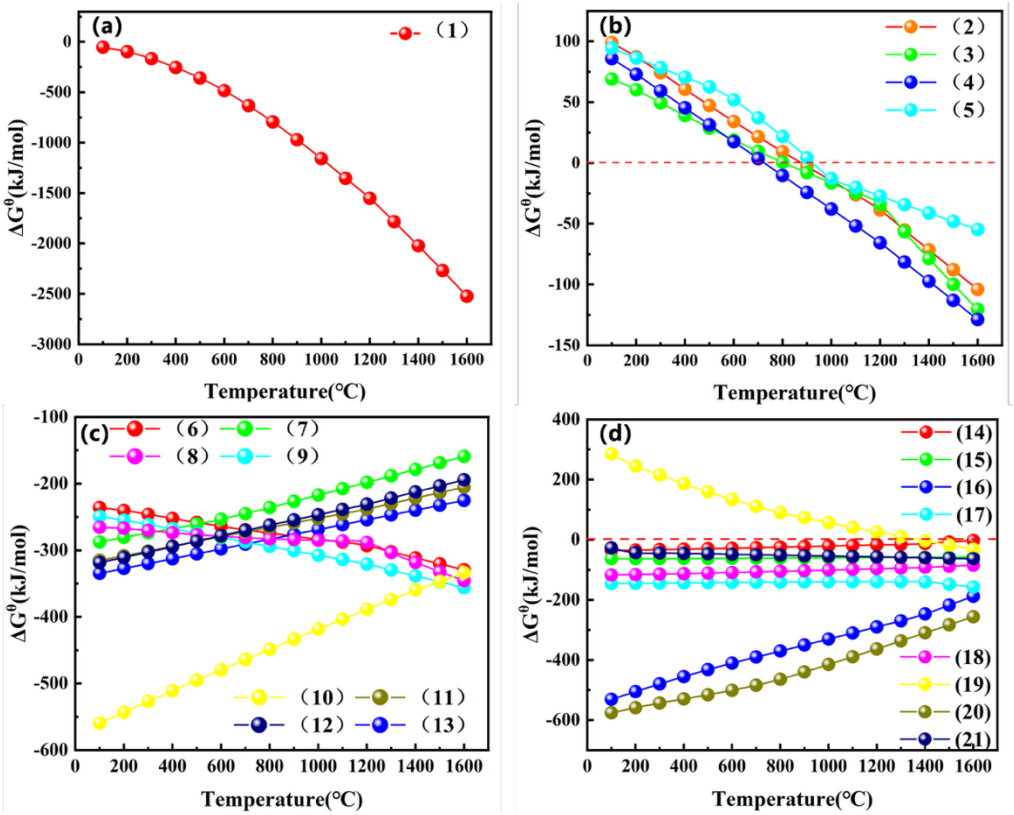


Fig. 3. Gibbs free energy variations during the matte smelting process: (a) Gibbs free energy change associated with pentlandite decomposition; (b) Gibbs free energy change during the decomposition stage; (c) Gibbs free energy change during the oxidation stage; (d) Gibbs free energy change during the slag formation stage

slag rises. This is because higher nickel matte grades require more oxygen injection, which increases the oxygen potential in the furnace and accelerates the formation of Fe_3O_4. As the nickel matte grade increases, the nickel content in the slag exhibits a gradual increase. This is because higher nickel matte grades accelerate the formation of Fe_3O_4 in the slag, increasing slag viscosity and reducing slag fluidity, which in turn raises the nickel content in the slag. If the nickel matte grade is too low, it will cause a series of problems such as insufficient thermal energy during the blowing process and operational difficulties, thereby increasing the cost of the blowing process. If the grade is too high, it will lead to increased nickel losses. Ultimately, the optimal nickel matte grade was determined to be 35%.

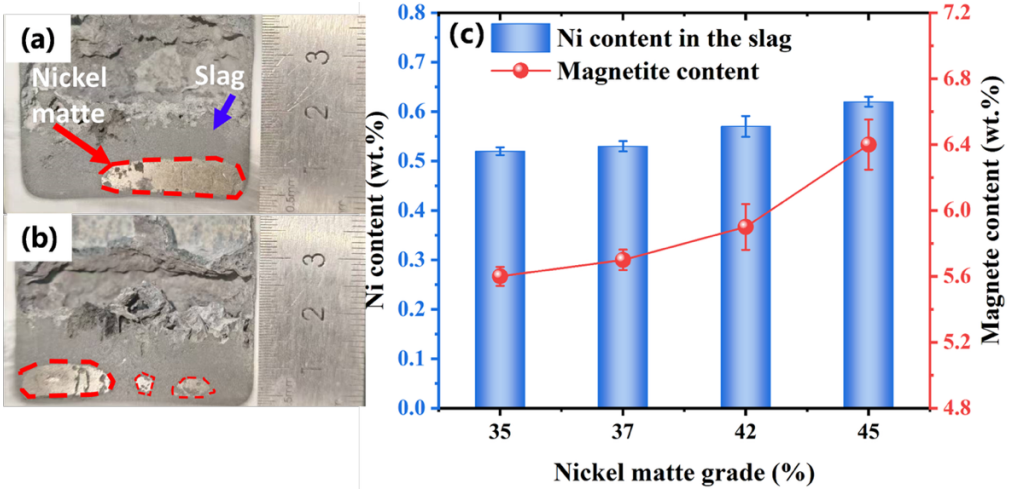


Fig. 4. Influence of nickel matte grade on nickel loss: (a)–(b) Cross-sectional morphologies of slag at different nickel matte grades ((a) Nickel matte grade of 35%, (b) Nickel matte grade of 45%); (c) Relationship among nickel matte grade, Fe_3O_4 content and nickel

3.3. Effect of temperature

The isothermal phase diagram of the quaternary SiO_2–FeO–CaO–MgO slag system with 16 wt.% MgO was generated through the phase equilibrium calculation function in FactSage 8.1, as presented in Fig. 5(a). With the increase of temperature, the area of the liquidus region expands continuously. Therefore, an increase in temperature promotes the advancement of the matte smelting operation. Thermodynamic equilibrium calculations were performed using FactSage 8.1 to determine the variation of phase assemblages with temperature at Fe/SiO_2 = 1.0 and CaO/SiO_2 = 0.1, as shown in Fig. 5(b). Elevated temperatures favor the formation of the low-melting liquid slag phase, while the mass fractions of high-melting phases, including spinel, anorthite ($CaAl_2Si_2O_8$), and olivine, exhibit a decreasing tendency. The variations of chemically dissolved nickel content and slag viscosity in nickel slag with temperature under the conditions of Fe/SiO_2 = 1.0, CaO/SiO_2 = 0.1 were calculated by using the thermodynamic simulation platform FactSage 8.1, as presented in Fig. 5(c). With the increase of temperature, the viscosity of slag decreases and the loss of chemically dissolved nickel in slag increases. This is because the rise in temperature enlarges the proportion of liquid slag phase, improves slag fluidity, and reduces slag viscosity; meanwhile, the oxygen utilization efficiency is enhanced, promoting more nickel to be oxidized into NiO and dissolved in the slag. Thermodynamic calculation results indicate that increasing temperature can reduce the loss of mechanically entrained nickel in slag, but it will raise the loss of chemically dissolved nickel in slag.

The nickel matte grade is controlled at approximately 35%, with Fe/SiO_2 = 1.0 and CaO/SiO_2 = 0.1. The sectional microstructural features of nickel slag samples obtained at 1400 ℃ and 1450 ℃ are depicted in Fig. 5(d) and Fig. 5(e), respectively. At 1400 ℃, the enrichment effect of nickel matte in slag is evidently inferior to that at 1450 ℃, indicating that increasing temperature is favorable to the matte smelting process. The phase evolution of nickel slag at different temperatures was investigated through XRD measurements, as demonstrated in Fig. 5(f). The nickel slag at various temperatures is mainly composed of olivine phase and spinel phase. The mass fractions of olivine and spinel phases in nickel slag were determined by semi-quantitative analysis. The results show that when the temperature rises from 1400 ℃ to 1500 ℃, the mass fraction of olivine phase increases from 87.8% to 90.3%, while that of spinel phase decreases from 12.2% to 9.7%. The phenomenon can be attributed to the following effects: as the temperature rises, the reaction between FeO and SiO_2 to form Fe_2SiO_4 is promoted (Eq. (14)); as the temperature increases, the activity of FeS rises, making it easier for Fe_3O_4 to be decomposed by FeS into FeO, which then reacts with SiO_2 to produce Fe_2SiO_4 in a slag-forming reaction (Eq. (19)). Fig. 5(g) shows the XPS results of nickel slag at different temperatures. As the temperature increased from 1400 °C to 1500 °C, the Fe^{2+} content in the slag increased from 66.41% to 76.88%, while the Fe^{3+} content decreased from 33.59% to 23.12%. This trend is consistent with the XRD results. The XRD and XPS results show that increasing the temperature increases the proportion of the olivine phase and decreases the proportion of the spinel phase in the slag, which is consistent with the FactSage phase-equilibrium calculation results showing that increasing the temperature increases the mass fraction of the liquid slag phase and improves slag fluidity.

The relationships between temperature and the Fe_3O_4 content in the slag, mechanically entrained nickel, and total nickel content of the slag are shown in Fig. 5(h). With increasing temperature, the Fe_3O_4 content in the slag decreased from 7.45 wt.% to 3.05 wt.%. Meanwhile, the loss of mechanically entrained nickel in the slag decreased markedly from 1.63 wt.% to 0.035 wt.%, and the total nickel loss to the slag was reduced from 1.97 wt.% to 0.43 wt.%. This is attributed to the fact that raising the temperature allows more Fe_3O_4 to dissolve in the slag, resulting in a decrease in the solid-phase fraction of the slag, effectively lowering its viscosity, and decreasing mechanical inclusion losses of nickel during smelting, thereby reducing the nickel content in the slag. When the temperature increased from 1400 to 1425 °C, the Ni content in the slag decreased significantly from 1.97 wt.% to 0.94 wt.%, corresponding to a reduction of 1.03% over a temperature increase of 25 °C, with an average decrease of 0.041 wt.%/℃ Ni. When the temperature was further increased from 1425 to 1500 °C, the Ni content decreased from 0.94 wt.% to 0.43 wt.%, corresponding to a reduction of only 0.51% over a temperature increase of 75 °C, with an average decrease of approximately 0.0068 wt.%/℃ Ni. Although increasing the temperature can improve slag fluidity and reduce the Ni content in the slag, operation at higher temperatures requires greater heat input and consequently leads to increased energy consumption.

Therefore, further increasing the temperature above 1425 °C would result in a substantial increase in heat demand, while providing only a relatively limited additional reduction in the Ni content of the slag. Considering the trade-off between minimizing Ni losses and reducing energy consumption, 1425 °C was selected as the optimum temperature.

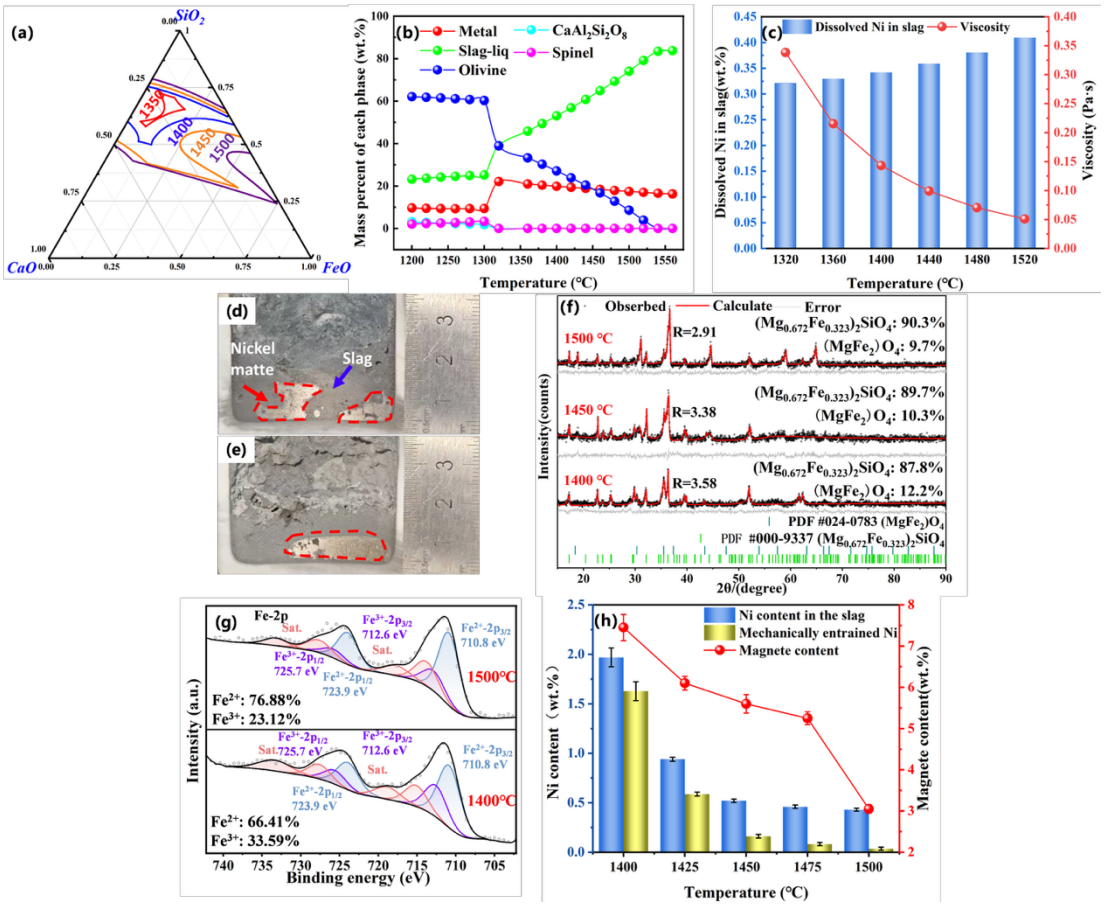


Fig. 5 Influence of temperature on nickel loss: (a) Isothermal phase diagram of the SiO_2–FeO–CaO–MgO quaternary system; (b) Relationship diagram between temperature and phase evolution; (c) Effect of temperature on viscosity and chemically dissolved nickel; (d)–(e) Cross-sectional micrographs of slag at different temperatures ((d) 1400 °C, (e) 1500 °C); (f) XRD patterns of nickel slag at different temperatures; (g) XPS spectra of nickel slag at different temperatures; (h) Relationship between Fe_3O_4 content, mechanically entrained Ni, and Ni content in slag and temperature

3.4. Effect of Fe/SiO_2 ratio

The phase evolution and the variation of chemically dissolved nickel loss in slag under different Fe/SiO_2 ratios were investigated using the equilibrium module of FactSage 8.1 software. Fig. 6(a) illustrates the variation of phase assemblages with the Fe/SiO_2 ratio. With the decrease of Fe/SiO_2 ratio, the proportion of solid olivine phase decreases obviously, while the mass fraction of slag liquid phase increases significantly. Fig. 6(b) illustrates the variation of chemically dissolved nickel with the Fe/SiO_2 ratio. The nickel loss associated with chemical dissolution in the slag decreases gradually as the Fe/SiO_2 ratio decreases. Thermodynamic analysis indicates that reducing the Fe/SiO_2 ratio can promote the matte smelting process of nickel sulfide concentrate.

The nickel matte grade was controlled at 35%, the smelting temperature at 1425 °C, and the CaO/SiO_2 ratio at 0.1. The sectional morphologies of nickel slag obtained at Fe/SiO_2 ratios of 0.9 and 0.7 are depicted in Fig. 6(c) and Fig. 6(d), respectively. The nickel slag enrichment effect was better when the Fe/SiO_2 ratio was 0.7 than when it was 0.9. This phenomenon occurs because a lower iron-to-silicon ratio causes SiO_2 to react with more FeO to form Fe_2SiO_4, which generates a greater amount

of liquid slag phase. This reduces the viscosity of the slag and facilitates its separation from the nickel matte.

The X-ray diffraction patterns of nickel slag obtained at different Fe/SiO_2 ratios are presented in Fig. 6(e). The major phases identified in the slag are olivine, spinel, and diopside. According to XRD semi-quantitative analysis results, as the Fe/SiO_2 ratio decreases, the mass fraction of spinel in slag decreases from 11.8% to 8.2%, while the mass fraction of olivine phase increases from 88.2% to 91.8%. This phenomenon occurs because lowering the Fe/SiO_2 ratio promotes the reaction between SiO_2 and FeO to form Fe_2SiO_4 (Eq (14)) during the slag-forming stage, thereby increasing the proportion of the olivine phase. At the same time, a lower Fe/SiO_2 ratio also promotes the reaction of SiO_2 with FeS and Fe_3O_4 to form Fe_2SiO_4 during the slag-forming stage (Eq. (19)). Therefore, lowering the iron-to-silicon ratio promotes the formation of the olivine phase while suppressing the formation of the spinel phase. Fig. 6(f) and Fig. 6(g) illustrate the SEM-EDS characterization of nickel slag obtained under Fe/SiO_2 ratios of 0.9 and 0.7, respectively. The EDS results indicate that points 1, 2, and 6 are assigned to the nickel matte phase, points 3, 8, and 10 are associated with olivine, points 4 and 7 with spinel, and points 5 and 9 with the amorphous glass phase. In the slag, nickel matte is mainly encapsulated by the olivine phase or adhered around the olivine, diopside, and spinel phases. Meanwhile, part of nickel exists in the form of NiO and dissolves into the olivine phase, spinel phase, and amorphous glass phase. The chemical compositions at different points are shown in Table 4. As the Fe/SiO_2 ratio decreased from 0.9 to 0.7, the w_{Fe}/w_{Mg} ratio in the spinel phase decreased from 19.69 (Point 4) to 2.42 (Point 7). This result indicates that, with decreasing Fe/SiO_2, the relative Mg content in the spinel phase increased, while the relative Fe content decreased, suggesting that Fe was released from the spinel phase. The spinel content at a Fe/SiO_2 ratio of 0.9 is higher than that at 0.7. At this time, the olivine phase is mainly forsterite, and many nickel matte particles are encapsulated within the olivine matrix. When the Fe/SiO_2 ratio is reduced to 0.7, the proportion of spinel phase declines compared with the case at 0.9, and the quantity of nickel matte particles in nickel slag is also reduced. Fig. 6(h) shows the XPS results of nickel slag at different Fe/SiO_2 ratios. The results indicate that as the Fe/SiO_2 ratio decreased from 0.9 to 0.7, the Fe^{2+} content in the slag increased from 69.58% to 74.18%, while the Fe^{3+} content decreased from 30.42% to 25.82%. Based on XRD, SEM and XPS analyses, a lower Fe/SiO_2 ratio favors olivine formation, suppresses the precipitation of high-melting-point spinel, improves nickel slag fluidity, and consequently benefits the matte smelting operation. This is consistent with the FactSage equilibrium phase calculation results, which show that decreasing the Fe/SiO_2 ratio increases the mass fraction of the liquid slag phase and improves slag fluidity.

Fig. 6(i) shows the relationship between different Fe/SiO_2 ratios and the melting point as well as viscosity of the slag, as presented in the figure. With a reduction in the Fe/SiO_2 ratio from 0.9 to 0.7, the slag melting temperature decreases from 1223 °C to 1159 °C, accompanied by a decline in viscosity from 0.262 Pa·s to 0.218 Pa·s. This is attributed to the increased addition of SiO_2, which reacts with FeO and MgO in slagging reactions, generating a larger amount of liquid slag and consuming the high-melting-point Fe_3O_4. Consequently, the fluidity of the slag is improved, leading to a reduction in both the viscosity and the melting point of the slag.

Fig. 6(j) illustrates the variations in the Fe_3O_4 content of the slag, mechanically entrained nickel, and total nickel content of the slag as a function of the Fe/SiO_2 ratio. As the Fe/SiO_2 ratio decreased, the Fe_3O_4 content in the slag, the amount of mechanically entrained nickel, and the total nickel content of the slag all exhibited a continuous downward trend. This is attributed to the fact that decreasing the Fe/SiO_2 ratio favors the formation of Fe_2SiO_4 while suppressing the generation of Fe_3O_4. The reduction in Fe_3O_4 content lowers the slag viscosity, improves the slag–matte separation environment, and reduces the mechanical entrainment loss of nickel in the slag. When the Fe/SiO_2 ratio decreased from 0.9 to 0.8, the nickel content in the slag decreased from 0.90 wt.% to 0.44 wt.%, corresponding to a reduction of 0.46%. When the Fe/SiO_2 ratio was further decreased from 0.8 to 0.7, the Ni content in the slag decreased to 0.24 wt.%, representing a further reduction of only 0.20%. This indicates that the marginal benefit of further decreasing the Fe/SiO_2 ratio becomes progressively smaller. Meanwhile, a lower Fe/SiO_2 ratio requires a greater addition of quartz. When the Fe/SiO_2 ratio decreased from 0.8 to 0.7, the required additional SiO_2 increased from 6.75 g to 10.45 g, corresponding to an approximately 54.81% increase in quartz addition. This not only increases flux consumption but also leads to a greater

amount of slag generation, thereby increasing the slag burden during the smelting process. Therefore, considering both Ni loss and the resulting slag burden, an Fe/SiO_2 ratio of 0.8 was selected as the optimum value.

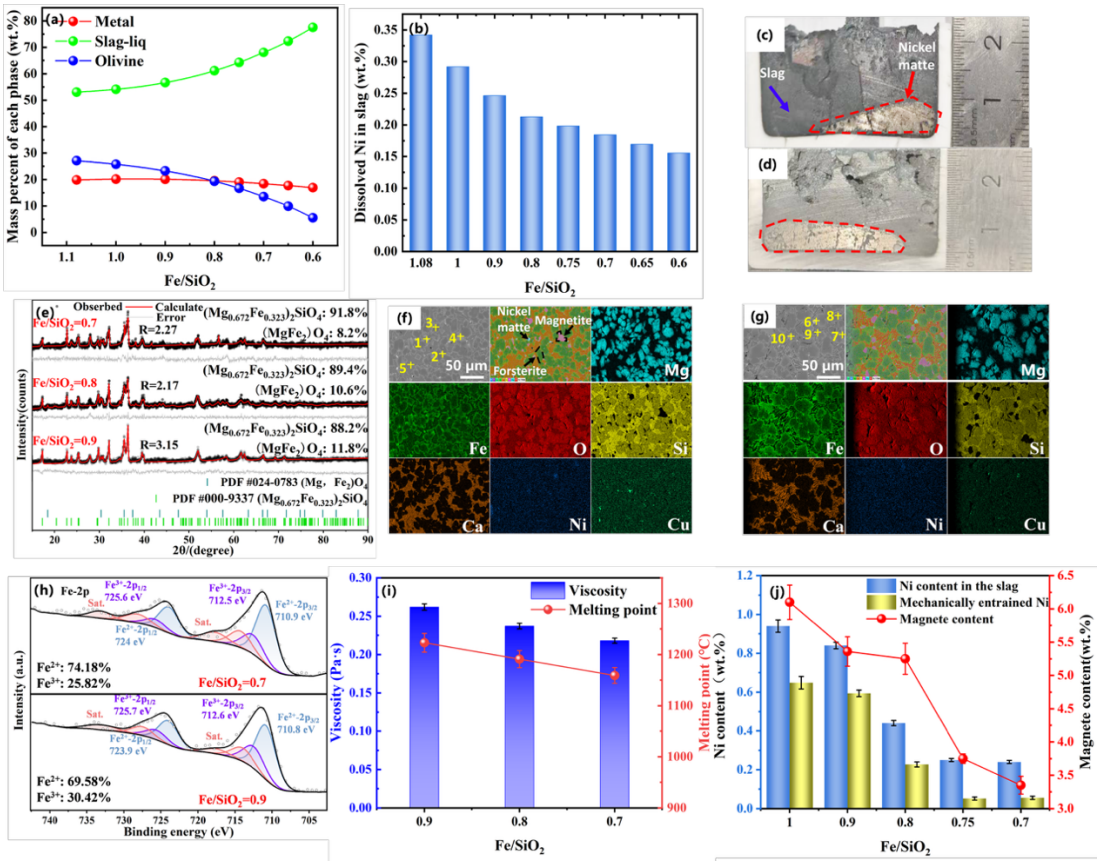


Fig. 6. Influence of different Fe/SiO_2 ratios on nickel loss: (a) Effect of different Fe/SiO_2 ratios on phase evolution; (b) Effect of different Fe/SiO_2 ratios on chemically dissolved nickel; (c)–(d) Cross-sectional micrographs of slag samples prepared with Fe/SiO_2 ratios of 0.9 and 0.7: (c) Fe/SiO_2 = 0.9, (d) Fe/SiO_2 = 0.7.; (e) XRD patterns of nickel slag samples corresponding to various Fe/SiO_2 ratios; (f)–(g) SEM-EDS images of nickel slag under different Fe/SiO_2 ratio conditions ((f) Fe/SiO_2 = 0.9, (g) Fe/SiO_2 = 0.7); (h) XPS spectra of nickel slag at different Fe/SiO_2 ratios; (i) Effect of different Fe/SiO_2 ratios on the melting point and viscosity of slag; (j) Relationship between Fe_3O_4 content, mechanically entrained Ni, and Ni content in slag and the Fe/SiO_2 ratio

Table 4. Chemical compositions (wt.%) of different points

Point	Cu	Ni	Fe	S	O	Si	Mg	Ca	Al
1	0.23	2.03	62.67	33.54	1.2	0.17	0.08	0.06	0.02
2	11.34	22.35	36.67	27.57	1.72	0.21	0.10	0.03	-
3	-	0.58	20.02	-	32.64	20.68	25.74	0.24	0.09
4	-	0.08	50.79	-	25.49	0.29	2.58	0.08	20.68
5	-	0.13	29.26	0.55	30.23	22.01	0.82	13.83	3.18
6	4.40	1.98	57.50	34.54	1.29	0.18	0.08	0.02	0.01
7	0.39	0.39	23.04	-	39.78	0.32	9.53	0.01	26.94
8	-	0.63	21.72	-	31.97	20.21	25.20	0.15	0.14
9	-	0.24	3.13	-	39.04	25.39	0.16	13.96	18.08
10	-	0.06	44.68	-	28.03	17.14	9.65	0.32	0.11

3.5. Effect of CaO/SiO_2 ratio

Using FactSage 8.1 thermodynamic calculations, the phase relationships of the SiO_2–FeO–MgO–CaO quaternary slag system were established, and the effect of varying CaO contents on the slag liquid

region was evaluated, as presented in Fig. 7(a). With the CaO content increasing from 3% to 11%, the liquid-phase field of the slag continuously expands. The effect of CaO/SiO_2 ratio on slag equilibrium phase assemblages was evaluated using FactSage 8.1 thermodynamic calculations, as presented in Fig. 7(b). As the CaO/SiO_2 ratio rises, the fraction of solid olivine in the slag gradually declines, whereas the proportion of the liquid phase increases continuously. The effect of CaO/SiO_2 ratio on chemically dissolved nickel is presented in Fig 7(c). Upon increasing the CaO/SiO_2 ratio, the chemically dissolved nickel content in slag shows a non-monotonic variation, initially decreasing and subsequently increasing. The loss of nickel in the oxidized state reaches the minimum at CaO/SiO_2 = 0.2. The thermodynamic analysis indicates that adding an appropriate amount of CaO can improve slag fluidity during matte smelting and facilitate slag–matte separation.

The nickel matte grade was controlled at approximately 35%, the smelting temperature was set at 1425 ℃, and the Fe/SiO_2 ratio was fixed at 0.8. Fig. 7(d) shows the XRD patterns of the slag samples at different CaO/SiO_2 ratios. The slag mainly consisted of olivine, spinel, and diopside phases. According to the semi-quantitative XRD analysis, as the CaO/SiO_2 ratio increased from 0.10 to 0.15, the mass fraction of the olivine phase decreased from 89.4% to 77.4%, while the mass fraction of the spinel phase decreased from 10.6% to 2.8%, and that of the diopside phase increased to 19.5%. This can be attributed to the reactions of FeO and MgO bearing components with CaO, promoting the formation of hedenbergite and diopside and consequently decreasing the proportion of the olivine phase while increasing that of the diopside phase. Meanwhile, under oxygen-enriched conditions, CaO can react with Fe_3O_4 to form $CaFe_2O_4$ (Eq. (20)), thereby decreasing the proportion of the spinel phase. When the CaO/SiO_2 ratio was further increased to 0.30, the mass fraction of the diopside phase increased to 54.5%, while that of the olivine phase decreased to 30.1%. In contrast, the spinel fraction increased again to 15.4%. This may be attributed to the reaction between excessive CaO and Fe_2SiO_4 to form $CaFeSi_2O_6$, accompanied by the release of a substantial amount of free FeO (Eq. (21)). Under the oxygen-enriched conditions, the released FeO is more readily oxidized by O_2 to Fe_3O_4, leading to an increase in the spinel content. Fig. 7(e) shows the XPS results of the slag at CaO/SiO_2 ratios of 0.1, 0.2, and 0.3. As the CaO/SiO_2 ratio increased from 0.1 to 0.3, the Fe^{2+} content in the nickel slag first increased and then decreased (70.38% → 71.75% → 67.74%), while the Fe^{3+} content first decreased and then increased (29.62% → 28.25% → 32.26%). Fig. 7(f)–7(h) displays the SEM-EDS micrographs of slag samples obtained with CaO/SiO_2 ratios of 0.1, 0.2, and 0.3, respectively. The EDS analysis results indicate that points 1, 6, 7, and 11 are associated with the nickel matte phase, points 2, 3, 8, and 12 with olivine, points 4, 9, 13, and 14 with spinel, and points 5, 10, and 15 with the amorphous glass phase. The corresponding chemical compositions are summarized in Table 5. Phase characterization demonstrates that nickel matte, olivine, spinel, and amorphous glass constitute the major phases of the nickel slag. The olivine phase consists primarily of forsterite and fayalite, with fayalite enclosing forsterite. The spinel phase is mainly a solid solution of Fe_3O_4 and magnesium ferrite $MgFe_2O_4$. The nickel matte phase is predominantly enclosed by the forsterite phase and attached around the olivine, spinel, and glass phases. Additionally, a portion of nickel is dissolved in the form of NiO within the olivine, spinel, and glass phases. Under a CaO/SiO_2 ratio of 0.1, a larger amount of spinel phase is present, and the nickel matte particles are relatively coarse, the w_{Fe}/w_{Mg} ratio in the spinel phase was 5.2 (Point 4). Upon increasing the CaO/SiO_2 ratio to 0.2, the contents of nickel matte and spinel phases in the slag decrease significantly relative to those at CaO/SiO_2 = 0.1, The w_{Fe}/w_{Mg} ratio in the spinel phase decreased to 2.37 (Point 9), indicating that Fe was released from Fe_3O_4. This phenomenon occurs because CaO reacts with Fe_3O_4 to form slag, thereby consuming the latter. Furthermore, increasing CaO addition promotes the expansion of the liquid slag phase and enhances Fe_3O_4 dissolution into the melt. The slag then becomes less viscous, improving the conditions for slag-matte separation and reducing the nickel matte phase in the slag. As the CaO/SiO_2 ratio further increases to 0.3, the nickel matte particles become coarser compared with those at CaO/SiO_2 = 0.2, indicating that the detrimental effect of CaO on smelting becomes dominant, at this point, the w_{Fe}/w_{Mg} ratios in the spinel phase changed to 1.24 (Point 13) and 2.74 (Point 14), indicating that part of the Fe re-entered the spinel phase. This is manifested as follows: excessive CaO destroys a large amount of the Fe_2SiO_4 structure, releasing substantial FeO, which is more readily oxidized by O_2 to form Fe_3O_4. Meanwhile, the high-melting-point Mg_2SiO_4 is exposed, and Mg^{2+} more easily combines with Fe^{3+} and O^{2-} to form $MgFe_2O_4$. Consequently, an increased

Table 5. Chemical compositions (wt.%) of different points

Point	Cu	Ni	Fe	S	O	Si	Mg	Ca	Al
1	5.21	16.86	37.59	33.83	4.97	0.26	0.19	1.03	0.06
2	-	0.16	33.48	-	38.41	16.96	10.62	0.26	0.11
3	-	0.28	17.33	-	41.61	18.41	21.97	0.20	0.21
4	-	0.39		-	36.22	1.60	5.87	0.17	25.22
5	-	-	16.29	-	41.50	23.55	0.98	11.85	5.83
6	57.86	1.17	5.79	12.40	10.38	6.77	0.36	3.58	2.79
7	68.91	-	5.80	16.22	7.29	2.37	0.65	0.99	0.77
8	-	0.26	7.60	-	48.30	17.73	25.68	0.21	0.22
9	-	0.26	20.84	-	43.29	0.28	8.78	0.04	26.51
10	-	0.15	23.59	-	32.78	21.32	0.69	13.67	7.80
11	8.93	0.86	51.65	32.48	0.13	1.28	0.22	0.94	0.49
12	-	0.13	3.61	-	52.62	17.28	25.90	0.26	0.19
13	-	0.02	10.38	-	53.32	0.25	8.35	0.02	27.48
14	-	-	14.88	-	54.16	0.28	5.43	0.09	25.18
15	-	0.04	15.06	-	36.97	20.57	2.29	17.15	7.92

increased spinel fraction leads to higher slag viscosity and greater entrainment of nickel matte within the slag. When CaO/SiO_2 increased from 0.10 to 0.15, the observations obtained by XRD, XPS, and SEM–EDS were consistent with the equilibrium phase calculation results, which showed that an increase in the liquid-phase fraction of the slag could improve slag fluidity. However, when CaO/SiO_2 was further increased to 0.30, the mass fraction of the spinel phase in the slag increased, adversely affecting slag fluidity, which deviated from the theoretical calculation results. This discrepancy is attributed to the assumption of complete thermodynamic equilibrium in the FactSage calculations, which cannot fully reflect the kinetic effects, local compositional variations, and crystallization during cooling in the actual smelting process. Therefore, FactSage has certain limitations in predicting the equilibrium phase assemblage at high CaO/SiO_2 ratios.

The phase transformation mechanism of the slag under different CaO/SiO_2 ratios is illustrated in Fig. 7(l). At a CaO/SiO_2 ratio of 0.1, Mg_2SiO_4 is enclosed by Fe_2SiO_4, and the spinel phase is mainly composed of a solid solution of Fe_3O_4 and $MgFe_2O_4$. Upon reaching a CaO/SiO_2 ratio of 0.2, CaO destabilizes Fe_2SiO_4, resulting in FeO release and subsequent formation of $CaFeSi_2O_6$ through reactions with CaO and SiO_2. Mg_2SiO_4 gradually becomes exposed, and Fe_3O_4 simultaneously decreases due to its destruction by CaO. When the CaO/SiO_2 ratio is further increased to 0.3, a large amount of Fe_2SiO_4 is decomposed, releasing more Fe^{2+}, which is more readily oxidized by O_2 to Fe^{3+}, thereby promoting the formation of Fe_3O_4. Meanwhile, Mg_2SiO_4 becomes completely exposed, and Mg^{2+} more easily combines with Fe^{3+} and O^{2-} to form $MgFe_2O_4$.

The FTIR profiles of nickel slag samples prepared with varying CaO/SiO_2 ratios are presented in Fig. 7(i). The characteristic absorption peaks near 490 cm^{-1}, 875 cm^{-1}, 920 cm^{-1}, 970 cm^{-1}, and 1045 cm^{-1} correspond to the bridging oxygen (Si–O–Si), Q^0–$[SiO_4]^{4-}$, Q^1–$[Si_2O_7]^{6-}$, Q^2–$[Si_2O_6]^{4-}$, and Q^3–$[Si_2O_5]^{2-}$ species, respectively, the characteristic absorption peak near 590 cm^{-1} arises from the Fe–O bending vibration of Fe_3O_4 (Yao et al., 2025; Chang et al., 2021). With the increase of the CaO/SiO_2 ratio from 0.1 to 0.2, the infrared absorption peak intensities corresponding to the Si–O–Si and Fe–O bonds decrease, indicating that the complex network structure formed by $[SiO_4]^{4-}$ tetrahedra is simplified. This is attributed to the dissociation of CaO, which generates a high concentration of O^{2-} ions that break the bridging oxygen bonds in the silicate network, thereby reducing the degree of polymerization of $[SiO_4]^{4-}$ tetrahedra. Consequently, the vibrational intensities of both Si–O–Si and Fe–O bonds decrease simultaneously due to structural disordering, leading to a simplified slag structure. Upon increasing the CaO/SiO_2 ratio from 0.2 to 0.3, the absorption peak intensity corresponding to Q^0 species decreases, while those corresponding to Q^2, Q^3, Si–O–Si, and Fe–O bonds increase. This is attributed to the reaction of CaO with oxides such as FeO, MgO, and SiO_2 in the system to form crystalline phases like diopside, which promotes the reconstruction of the silicate network into a more stable ordered structure. Consequently, the degree of ordering of $[SiO_4]^{4-}$ tetrahedra increases, and the vibrational coupling

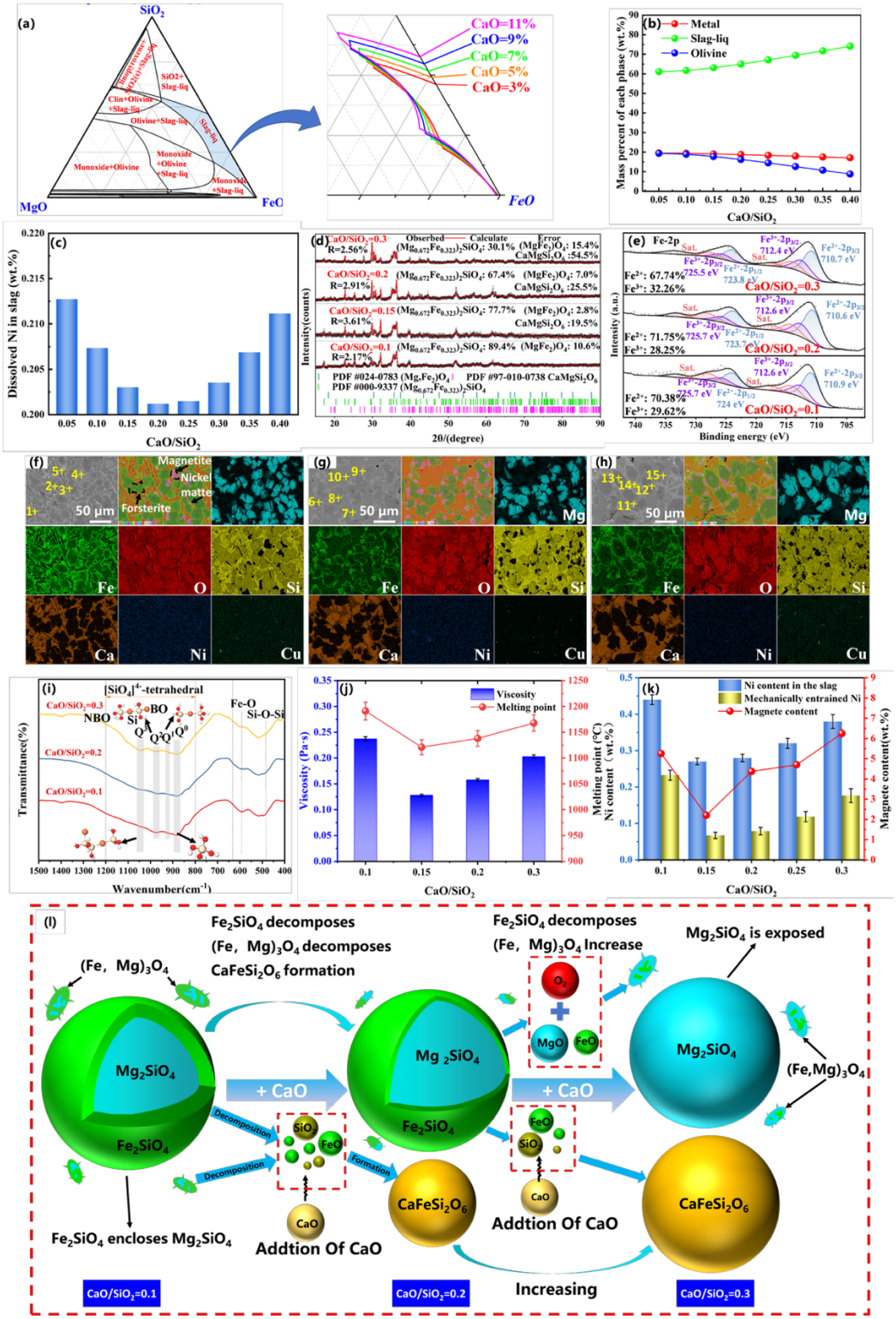


Fig. 7 Influence of different CaO/SiO_2 ratios on nickel loss: (a) Liquidus area of the SiO_2–FeO–MgO–CaO quaternary slag system as a function of CaO content; (b) Effect of different CaO/SiO_2 ratios on phase assemblage; (c) Effect of different CaO/SiO_2 ratios on chemically dissolved nickel; (d) XRD profiles of nickel slag under various CaO/SiO_2 ratios; (e) XPS spectra of nickel slag at different CaO/SiO_2 ratios; (f)–(h) SEM-EDS images of nickel slag under different CaO/SiO_2 ratios ((f) CaO/SiO_2 = 0.1, (g) CaO/SiO_2 = 0.2, (h) CaO/SiO_2 = 0.3); (i) FTIR spectra of nickel slag at different CaO/SiO_2 ratios; (j) Relationship between CaO/SiO_2 ratio and slag melting point as well as viscosity; (k) Relationship between Fe_3O_4 content, mechanically entrained Ni, and Ni content in slag and the CaO/SiO_2 ratio; (l) Phase transformation mechanism diagram of nickel slag at different CaO/SiO_2 ratios

of Si–O–Si and Fe–O bonds intensifies, resulting in stronger absorption peaks and a more complex slag structure (Park et al., 2011; Zhu et al., 2025). A moderate adjustment of CaO/SiO_2 from 0.1 to 0.2 contributes to the simplification of the slag structure.

The relationship between different CaO/SiO_2 ratios and the melting point as well as viscosity of the slag is shown in Fig. 7(j). Upon increasing the CaO/SiO_2 ratio from 0.1 to 0.15, the slag melting temperature decreases from 1191°C to 1128°C, while its viscosity is reduced from 0.237 Pa·s to 0.128 Pa·s. This is attributed to the fact that a small amount of CaO participates in slagging reactions with FeO, MgO, and SiO_2, forming a larger amount of liquid slag phase. Meanwhile, CaO disrupts the complex silicate structure in the slag, thereby lowering its melting point and viscosity. When the CaO/SiO_2 ratio reaches 0.3, both the slag melting temperature and viscosity increase, reaching 1168°C and 0.203 Pa·s, respectively. This is attributed to the fact that excessive CaO destroys a large amount of the fayalite structure, releasing more Fe^{2+}, which is more readily oxidized by O_2 to form high-melting-point Fe_3O_4. Meanwhile, the forsterite originally encapsulated by fayalite becomes exposed, and MgO more easily combines with Fe_2O_3 to form high-melting-point $MgFe_2O_4$. Consequently, the increased proportion of refractory phases leads to higher slag melting temperature and viscosity. The relationships between the CaO/SiO_2 ratio and the Fe_3O_4 content in the slag, mechanically entrained nickel, and total nickel content of the slag are shown in Fig. 7(k). With increasing CaO/SiO_2 ratio, the Fe_3O_4 content in the slag, mechanically entrained nickel, and the total nickel content of the slag initially decreased and subsequently increased, reaching their minimum values at a CaO/SiO_2 ratio of 0.15. This indicates that an appropriate addition of CaO facilitates slag–matte separation and reduces mechanical inclusion losses of nickel in the slag. Since the nickel content in the slag reached its minimum at a CaO/SiO_2 ratio of 0.15, this ratio was selected as the optimum CaO/SiO_2 ratio.

Based on the single factor experiments, the optimal conditions were determined to be a target matte grade of approximately 35%, a smelting temperature of 1425 °C, Fe/SiO_2 = 0.8, and CaO/SiO_2 = 0.15. Under these experimental conditions, the measured Ni content in the slag was 0.27 wt.%. To further characterize the products obtained under these conditions, the overall chemical compositions of the matte and slag were analyzed, and the results are summarized in Table 6. As shown in the table, the matte obtained under the optimal conditions had a grade of 34.55% (20.52% Ni and 14.03% Cu), corresponding to a deviation of only 0.45% from the target matte grade of 35%. Based on the measured masses of the matte and slag products, approximately 94.96% of Ni, 95.86% of Cu, and 72.91% of Co were distributed to the matte phase, whereas 5.04% of Ni, 4.14% of Cu, and 27.09% of Co remained in the slag phase. These results demonstrate the successful implementation of the matte smelting process for high-magnesia nickel sulfide ore.

Table 6. Chemical compositions of the slag and nickel matte under optimal conditions

Nickel	Ni		Cu		Co		Fe		S	Other
Matte	20.52		14.03		0.38		33.69		30.63	0.75
Slag	Ni	Cu	Co	Fe	S	CaO	MgO	SiO_2	Al_2O_3	Other
	0.27	0.14	0.04	30.02	0.12	6.27	16.87	36.52	6.79	2.96

4. Conclusions

In summary, this study investigates the slag composition regulation during the matte smelting of nickel sulfide concentrate with a MgO content of 13.66 wt.%, elucidates the reaction mechanisms of the matte smelting process, and examines the evolution of phases, physical properties, and nickel content in the nickel slag under various parameter conditions. The optimal process parameters for smelting high-magnesium nickel sulfide concentrate are obtained, ultimately ensuring that the nickel content in the slag meets industrial production targets. The conclusions are as follows:

a. The reaction mechanisms of the matte smelting process for nickel sulfide concentrate can be divided into three main stages: the decomposition stage, the oxidation stage, and the slag-forming stage. During the decomposition stage, the primary reactions involve the decomposition of various sulfide minerals. In the oxidation stage, the main reactions involve the conversion of sulfide minerals and the subsequent oxidation of sulfides such as Ni_3S_2, FeS, and Cu_2S formed during the decomposition

stage. The slag-forming stage is characterized by reactions in which FeO, MgO, CaO, and other oxides combine with SiO_2 to form silicates.

b. As the nickel matte grade increases, the Fe_3O_4 fraction within the slag rises, resulting in higher viscosity and deteriorated slag–matte separation conditions. With increasing temperature, the fraction of solid particles within the slag decreases, the mass fraction of the slag liquid phase increases, the Fe_3O_4 content in the slag decreases, and slag viscosity decreases, leading to a reduction in the nickel content of the slag.
c. A lower Fe/SiO_2 ratio promotes the formation of a larger liquid fraction, reduces Fe_3O_4 concentration, decreases the melting temperature and viscosity of the slag, minimizes nickel loss caused by mechanical entrainment, and ultimately lowers the residual nickel level in the slag. Appropriately increasing the CaO/SiO_2 ratio can simplify the slag structure, lower its melting temperature and viscosity, reduce the loss of nickel due to mechanical entrapment in the slag, and decrease the nickel content in the slag; however, an excessively high CaO/SiO_2 ratio will cause the slag structure to become complex again, resulting in higher melting temperature and viscosity, an increase in the loss of nickel due to mechanical entrapment in the slag, and an increase in the nickel content in the slag.
d. Under the conditions of a nickel matte grade of 35%, a temperature of 1425 °C, a Fe/SiO_2 ratio of 0.8, and a CaO/SiO_2 ratio of 0.15, the nickel content in the slag is 0.27 wt.%, which meets the requirements of practical industrial production.

Acknowledgements

This work was supported by Yunnan Fundamental Research Projects (No. 202501BN070001-013, 202501AU070114), Open Project of the National Key Laboratory of New Technologies for Enhanced Metallurgy of Nonferrous Metals (No. YSQH-ZD-25003), Yunnan Fundamental Research Projects (No. 202401BE070001-032, 202501AV070004).

References

BOŽINOVIĆ K., ŠTRBAC N., MITOVSKI A., SOKIĆ M., MINIĆ D., MARKOVIĆ B., STOJANOVIĆ J., 2011. *Thermal decomposition and kinetics of pentlandite-bearing ore oxidation in the air atmosphere.* Metals, 11, 1364.

CHANG Y.E., LIN C.M., SHEN J.M., CHANG W.T., WU W., 2021. *Effect of MgO content on the viscosity, foaming life, and bonding in liquid for the CaO-SiO2-MgO-5Al2O3-30FeO slag system.* Metals, 11, 249.

ELSHKAKI A., RECK B.K., GRAEDEL T.E., 2017. *Anthropogenic nickel supply, demand, and associated energy and water use.* Resources, Conservation and Recycling, 125, 300–307.

FARIS N., POWNCEBY M.I., BRUCKARD W.J., CHEN M., 2022. *The direct leaching of nickel sulfide flotation concentrates – A historic and state-of-the-art review part I: Piloted processes and commercial operations.* Mineral Processing and Extractive Metallurgy Review, 44, 407–435.

FENG B., WANG P.C., LU Y.P., FENG Q.M., 2016. *Role of sodium hexametaphosphate in flotation of a nickel ore.* Physicochemical Problems of Mineral Processing, 52, 170–181.

HENAO H.M., HINO M., ITAGAKI K., 2002. *Phase equilibrium between Ni-S melt and CaO-Al2O3 based slag in CO-CO2-SO2 gas mixtures at 1773 K.* Materials Transactions, 43, 2873–2879.

LIN Q.Q., SUN L., CAO Y., GUO Y.H., LIANG M.H., LU B., SU X.H., SUN W., 2025. *Stepwise separation of highly altered copper-nickel sulfide ores utilizing structural characteristics and magnetic response for enhanced recovery.* Separation and Purification Technology, 382, 135893.

LU W.J., YUAN Z.T., LIU J.T., LI L.X., WANG N.L., MENG Q.Y., 2017. *Selective agglomeration of magnetite in pentlandite-serpentine system and implication for their separation.* Physicochemical Problems of Mineral Processing, 53, 943–955.

MU W., HUANG Z., XIN H., LUO S., ZHAI Y., XU Q., 2019. *Extraction of copper and nickel from low-grade nickel sulfide ore by low-temperature roasting, selective decomposition and water-leaching process.* JOM, 71, 4647–4657.

MUDD G.M., 2010. *Global trends and environmental issues in nickel mining: Sulfides versus laterites.* Ore Geology Reviews, 38, 9–26.

PARK H.S., PARK S.S., SOHN I., 2011. *The viscous behavior of FeOt-Al2O3-SiO2 copper smelting slags.* Metallurgical and Materials Transactions B, 42, 692–699.

PISKUNEN P., AVARMAA K., O'BRIEN H., KLEMETTINEN L., JOHTO H., TASKINEN P., 2017. *Precious metal distributions in direct nickel matte smelting with low-Cu mattes.* Metallurgical and Materials Transactions B, 49, 98–112.

QIN W.Q., ZHEN S.J., YAN Z.Q., CAMPBELL M., WANG J., LIU K., ZHANG Y.S., 2009. *Heap bioleaching of a low-grade nickel-bearing sulfide ore containing high levels of magnesium as olivine, chlorite and antigorite.* Hydrometallurgy, 98, 58–65.

SHEN Y.Y., CHONG J.K., HUANG Z.N., TIAN J.K., ZHANG W.J., TANG X.C., DING W., DU X., 2019. *Viscosity and structure of a CaO-SiO2-FeO-MgO system during a modified process from nickel slag by CaO.* Materials, 12, 2562.

SUKHOMLINOV D., VIRTANEN O., LATOSTENMAA P., JOKILAAKSO A., TASKINEN P., 2019. *Impact of MgO and K2O on slag-nickel matte equilibria.* Journal of Phase Equilibria and Diffusion, 40, 768–778.

SUN W., LI X., LIU R., ZHAI Q., LI J., 2021. *Recovery of valuable metals from nickel smelting slag based on reduction and sulfurization modification.* Minerals, 11, 1022.

WANG B.R., YANG H.Y., JIN Z.N., LIU Z.J., ZOU M.J., 2022. *Effect of Fe/SiO2 ratio and Fe2O3 on the viscosity and slag structure of copper-smelting slags.* Metals, 12, 24.

WANG F., LIU F., ELLIOTT R., REZAEI S., KHAJAVI L.T., BARATI M., 2020. *Solid state extraction of nickel from nickel sulfide concentrates.* Journal of Alloys and Compounds, 822, 153582.

WANG F.M., MARCUSON S., XU M.Q., WALKER M., BARATI M., 2024. *Extraction of nickel from ultramafic nickel sulfide concentrate by metallic iron addition.* Metallurgical and Materials Transactions B, 55, 3254–3265.

WANG G.H., CUI Y.R., LI X.M., YANG S.F., ZHAO J.X., TANG H.L., LI X.T., 2020. *Molecular dynamics simulation on microstructure and physicochemical properties of FexO-SiO2-CaO-MgO-"NiO" slag in nickel matte smelting under modulating CaO content.* Minerals, 10, 149.

WANG G.H., CUI Y.R., YANG J., LI X.M., YANG S.F., ZHAO J.X., TANG H.L., 2021. *Fe/SiO2 ratio on the properties, microstructure and Fe-containing phases of nickel matte smelting slag.* Metallurgical and Materials Transactions B, 52, 1463–1471.

WANG G.H., CUI Y.R., LI X.M., SHI R.M., YANG J., YANG S.F., ZHAO J.X., NAN J.F., 2023. *Structure and adaptability of FexO-SiO2-MgO-15 wt% CaO-0.026 wt% NiO slag with the Fe/SiO2 mass ratio of 1.2 in flash matte smelting.* Ceramics International, 49, 2531–2539.

YAO L.C., ZHANG H.P., LI B., ZHANG B., ZHU Y.F., WEI Y.G., ZHOU S.W., WANG H., 2025. *Investigation on cleaning copper slag using fly ash to recover matte.* Journal of Sustainable Metallurgy, 11, 1091–1103.

YU D.W., UTIGARD T.A., 2012. *TG/DTA study on the oxidation of nickel concentrate.* Thermochimica Acta, 553, 56–65.

ZHANG H.P., LI B., WEI YG., WANG H., YANG Y.D., 2022. *Effect of CaO on copper loss and phase transformation in copper slag.* Metallurgical and Materials Transactions B, 53, 1538–1551.

ZHANG X., LI X., WANG S., 2023. *Effect of B2O3 on the melting characteristics and slag-matte separation of nickel flash furnace melting.* JOM, 75, 3532–3544.

ZHAO K., GAO F., YANG Q., 2022. *Comprehensive review on metallurgical upgradation processes of nickel sulfide ores.* Journal of Sustainable Metallurgy, 8, 37–50.

ZHEN S.J., YAN Z.Q., ZHANG Y.S., WANG J., CAMPBELL M., QIN W.Q., 2009. *Column bioleaching of a low grade nickel-bearing sulfide ore containing high magnesium as olivine, chlorite and antigorite.* Hydrometallurgy, 94, 337–341.

ZHU Y.F., LI B., WEI YG., ZHOU S.W., WANG H., 2025. *Advanced approach to sustainable recovery of valuable metals via co-smelting of waste printed circuit boards with copper smelting slag.* Chemical Engineering Journal, 524, 169531.